LANGMUIR

Article

pubs.acs.org/Langmuir

Terbium-Doped VO_2 Thin Films: Reduced Phase Transition Temperature and Largely Enhanced Luminous Transmittance

Ning Wang,[†] Martial Duchamp,[‡] Rafal E. Dunin-Borkowski,[‡] Shiyu Liu,[§] XianTing Zeng,[§] Xun Cao,[†] and Yi Long*[,†]

[†]School of Materials Science and Engineering, Nanyang Technological University, 50 Nanyang Avenue, 639798 Singapore

[‡]Ernst Ruska-Centre for Microscopy and Spectroscopy with Electrons (ER-C) and Peter Grünberg Institute (PGI), Forschungszentrum Jülich, 52428 Jülich, Germany

[§]Singapore Institute of Manufacturing Technology, 71 Nanyang Drive, 638075 Singapore

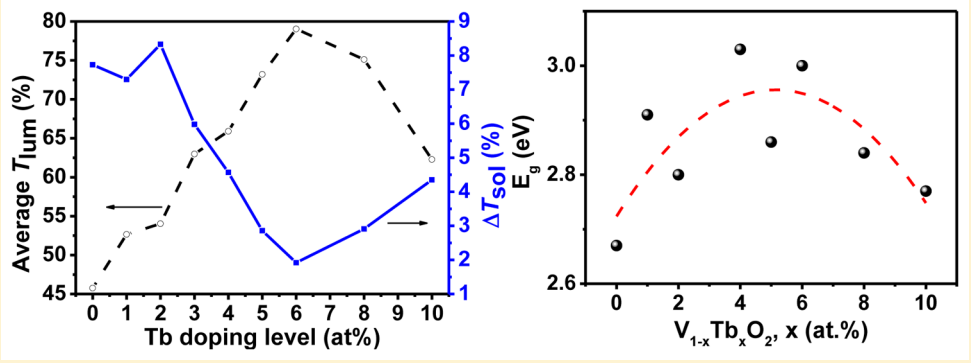

ABSTRACT: Vanadium dioxide (VO_2) is a well-known thermochromic material with large IR modulating ability, promising for energy-saving smart windows. The main drawbacks of VO_2 are its high phase transition temperature (τ_c = 68 °C), low luminous transmission (T_{lum}), and weak solar modulating ability (ΔT_{sol}). In this paper, the terbium cation (Tb^{3+}) doping was first reported to reduce τ_c and increase T_{lum} of VO_2 thin films. Compared with pristine VO_2, 2 at. % doping level gives both enhanced T_{lum} and ΔT_{sol} from 45.8% to 54.0% and 7.7% to 8.3%, respectively. The T_{lum} increases with continuous Tb^{3+} doping and reaches 79.4% at 6 at. % doping level, representing ~73.4% relative increment compared with pure VO_2. This has surpassed the best reported doped VO_2 thin films. The enhanced thermochromic properties is meaningful for smart window applications of VO_2 materials.

1. INTRODUCTION

Vanadium dioxide (VO_2) is a well-studied thermochromic material that undergoes fully reversible metal−insulator transitions (MIT). At the critical temperature (τ_c) of 68 °C,[1,2] VO_2 transforms from semiconducting monoclinic phase to metallic rutile phase, which can be reflected by a sharp change in infrared (IR) transmittance while visible light transmittance (T_{lum}) stays nearly constant. As its τ_c being the closest to the room temperature among transition metal oxides, while taking the advantage of being transparent at both states (hot metallic and cool insulating states) compared to the newly developed organic[3] and hybrid[4] smart systems based on temperature-responsive hydrogel matrices, VO_2 has since become the most potential choice to be applied in energy-saving smart windows[5−7] and other thermal/optical/sensing devices.[8−12]

VO_2 faces the drawback of both low T_{lum} and solar modulating ability (ΔT_{sol}, the ability to regulate the input solar energy). Simultaneously enhancing these properties has been achieved through casting VO_2 nanoparticles/matrix composite foils,[13,14] thin film nanostructuring such as bio-inspired VO_2 with antireflection (AR) effects,[15] and controlled nanoporosity.[16] By far, high τ_c is the most crucial issue that hinders the application of thermochromic smart windows, and the most efficient way to reduce τ_c is doping, although some dopants may degrade T_{lum}. Table 1 lists the selected dopants which can reduce τ_c. It is of interest to observe that most dopants have a certain upper limit in doping level to reduce τ_c. The reducing rate and the effects on T_{lum} are also summarized in this table.

Rare earth ions (RE^{3+}) have large ionic radii and rich valence shell electrons. Therefore, doping RE^{3+} into VO_2 crystal lattice could lead to appreciable extra strain energy via structure deformation and altered holes or electrons carrier density which may profit enhancing the thermochromic properties of VO_2.[27] In this work, we first report the Tb^{3+} doping in VO_2 lattice, and its effect on lowering down the τ_c and significantly increasing the T_{lum} has been investigated systematically.

Received: November 16, 2015
Revised: December 14, 2015
Published: January 4, 2016

 © 2016 American Chemical Society

DOI: 10.1021/acs.langmuir.5b04212
Langmuir 2016, 32, 759−764

Table 1. Effects of Selected Dopants on τ_c and T_{lum} of VO_2

dopant	limit (at. %)	effect on τ_c (°C/at. %)	effect on T_{lum}
Eu^{3+} [17]	4	−6.5	increased by 22% at 4 at.%
Mg^{2+} [18−20]	7	−3	increased by 11% at 7 at.%
W^{6+} [21]	2.5	−23	decreased by 10% at 2.5 at.%
F^{-} [21]	2.1	−20	unchanged
Mo^{6+} [22]	2.5	−12	decreased by 10% at 3 at.%
Nb^{5+} [22]	4	−8	decreased by 50% at 11 at.%
P^{3-} [23]	1	−13	not available
Fe^{3+}[24]	1.4	−6	not available
Sb^{3+} [25]	7	−1	35% at 3 at.%.
Zr^{4+} [26]	11	unchanged	increased by 65%

2. EXPERIMENTAL SECTION

The chemicals used in this study were vanadium(V) oxide (V_2O_5, 99.99%, Alfa Aesar), terbium oxide (Tb_2O_3, 99.99%, Alfa Aesar), hydrogen peroxide (H_2O_2, 30 wt %, VWR), and polyvinylpyrrolidone (PVP, 99%, Sigma-Aldrich). All of the chemicals were used as received without any further purification.

2.1. Synthesis of Tb-Doped VO_2 (M) Thin Films. 180 mg of V_2O_5 powder and required amount of Tb_2O_3 powder were added into 15 mL of H_2O_2 at 70 °C. After 10 min of stirring at 800 rpm, a vigorous exothermic reaction took place and formed a reddish-brown sol. The precursor was then cooled in an ice bath, and another 1 mL of H_2O_2 was added to dissolve any remaining Tb_2O_3 powder. 12 mg of PVP was subsequently added to improve the viscosity of the precursor, which was dip-coated onto a 15 × 15 × 0.5 mm^3 precleaned fused silica substrate using a dip coater (KSV Instruments) at a speed of 300 mm/min. The precursor film was annealed at 550 °C for 2 h in a tube furnace with argon (99.9995%, NOX) atmosphere, during which the ramping rate was set to 1.0 °C/min, and gas flow rate was tuned to ∼200 mL/min.

2.2. Characterization. The phases of the samples were determined with an XRD-6000 X-ray diffractometer (XRD, Shimadzu, Japan), of which the Cu Kα radiation was produced at 40 kV and 30 mA with $\lambda \approx 0.154\,06$ nm at an X-ray grazing angle of 1.0°. The surface morphology, roughness, and particle size analyses were examined using a Digital Instrument DI3100 atomic force microscope (AFM, Bruker, Germany) under tapping mode. The transmission electron microscope (TEM) characterization was performed with JEOL JEM-2010 with the accelerating voltage of 200 kV. The XPS data were collected in the V 2p and Tb 3d binding energy regions using a Thermo Scientific ESCALAB 250Xi XPS spectrometer (900 μm spot, 3 scans, 75 eV pass energy) equipped with Avantage Data System software. The transmittance spectra and hysteresis loop were collected using a Cary 5000 ultraviolet−visible light-near-infrared (UV−vis−NIR) spectrophotometer (Agilent, USA), which was equipped with a PE120 Peltier system simple heating and cooling stage (Linkam, UK). The calculations of integrated T_{lum} ($380 \le \lambda \le 780$ nm) and ΔT_{sol} ($280 \le \lambda \le 2500$ nm) can be found in eqs 1 and 2, respectively.

$$T_{lum/sol} = \int \varphi_{lum/sol}(\lambda) T(\lambda)\, d\lambda / \int \varphi_{lum/sol}(\lambda)\, d\lambda \quad (1)$$

$$\Delta T_{sol} = T_{sol}(20\ °C) - T_{sol}(90\ °C) \quad (2)$$

where $T(\lambda,\tau)$ is the recorded percentage transmittance at a particular wavelength and temperature, φ_{lum} is the standard luminous efficiency function for the photopic vision of human eyes,[28] and φ_{sol} is the solar irradiance spectrum for air mass 1.5 (corresponding to the sun standing 37° above the horizon).[29]

3. RESULTS AND DISCUSSION

3.1. Synthesis of Tb-Doped VO_2 Thin Films. Figure 1a shows the XRD patterns of the Tb-doped VO_2 thin films. As depicted, all of the samples ($V_{1-x}Tb_xO_2$, x = 0−10 at. %) exhibit the characteristic (011) peak at 2θ = ∼28°, revealing the formation of VO_2(M) phase (JCPDS #82-661). In addition, no other vanadium oxide phase peaks can be found in the patterns, which proves the high phase purity of the VO_2 thin films. The high-resolution XPS scan of V 2p and Tb 3d was performed in the binding energy ranges of 535−507 and 1287−1235 eV, respectively. As shown in Figure 1b, the V $2p_{3/2}$ peak can be split into two peaks located at 518.6 and 517.8 eV, which should be ascribed to the V^{5+} and V^{4+}, respectively. The existence of V^{5+} should be attributed to the partial oxidation of the thin film within several nanometers scale in the top layer. The Tb 3d peaks can be clearly observed in Figure 1c, and the Tb $3d_{3/2}$ and Tb $3d_{5/2}$ peaks locate at 1278.4 and 1243.4 eV, respectively. The calculated doping level of Tb^{3+} based on the XPS spectra of V 2p and Tb 3d is ∼10.3 at. %, in accordance with the stoichiometry of the sample $V_{0.9}Tb_{0.1}O_2$.

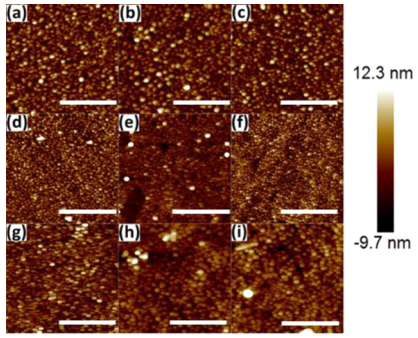

Figure 2. 2D AFM images in height of (a−g) 0−6 at. %, (h) 8 at. %, and (i) 10 at. % Tb-doped VO_2 thin films. The scan area of each image is 2 × 2 μm^2, and all of the scale bars represent 1 μm.

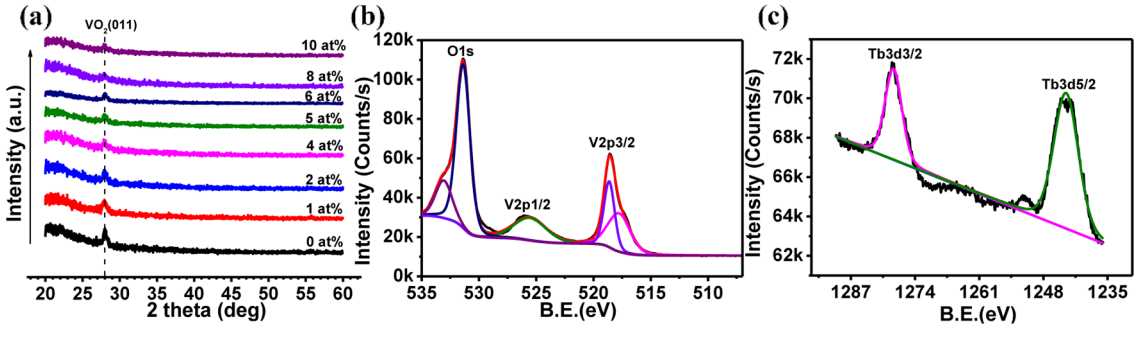

Figure 1. XRD patterns of Tb-doped VO_2 thin films (a). High-resolution XPS scan of V 2p (b) and Tb 3d (c) for the sample $V_{0.9}Tb_{0.1}O_2$.

DOI: 10.1021/acs.langmuir.5b04212
Langmuir 2016, 32, 759−764

Table 2. Summary of Experimental Results for Tb-Doped VO_2 Thin Films

		T_{lum} (%)			T_{sol} (%)					
doping level (at. %)	thickness[a] (nm)	20 °C	90 °C	ΔT_{lum} (%)	20 °C	90 °C	ΔT_{sol} (%)	τ_c (°C)	$\Delta\tau_c$ (°C)	grain size[b] (nm)
0	100	44.5	47.1	−2.6	51.6	43.9	7.7	67.5	15	60.7
1	100	52.0	53.3	−1.3	57.1	49.8	7.3	67.5	15	60.0
2	100	53.4	54.7	-1.3	58.7	50.3	8.3	65.0	20	61.5
4	100	65.4	66.4	−1.0	68.1	63.5	4.6	62.5	15	71.0
5	100	72.8	73.6	−0.8	74.6	71.7	2.9	60.0	10	60.1
6	100	78.6	79.5	−0.9	79.4	77.5	1.9	67.5	15	57.5
8	100	74.8	75.4	−0.6	76.4	73.5	2.9	72.5	35	73.6
10	100	61.3	63.3	−2.0	65.4	61.1	4.4	67.5	15	97.8

[a]The thickness derivation is within 10 nm. [b]The mean grain sizes were obtained from the respective AFM images.

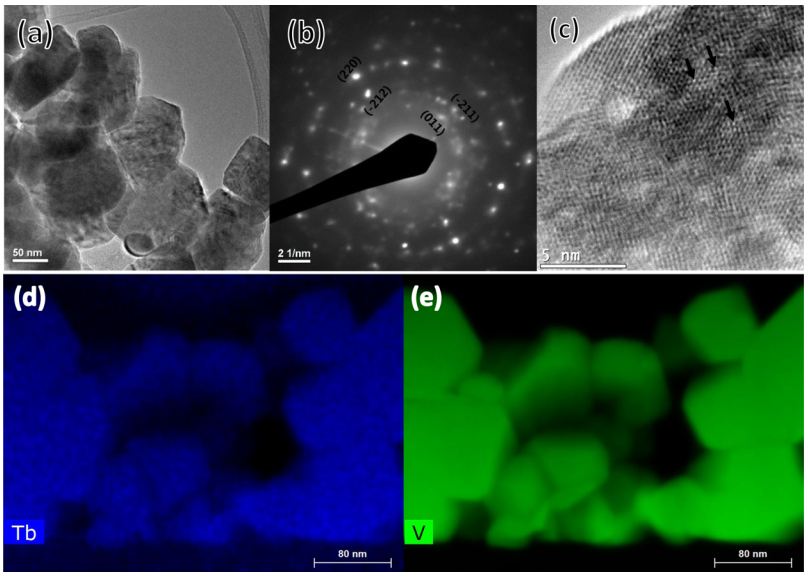

Figure 3. TEM image (a), SAED pattern (b), and the HRTEM (c) for the sample $V_{0.98}Tb_{0.02}O_2$. (d) and (e) are the EDX mapping of Tb and V elements, respectively.

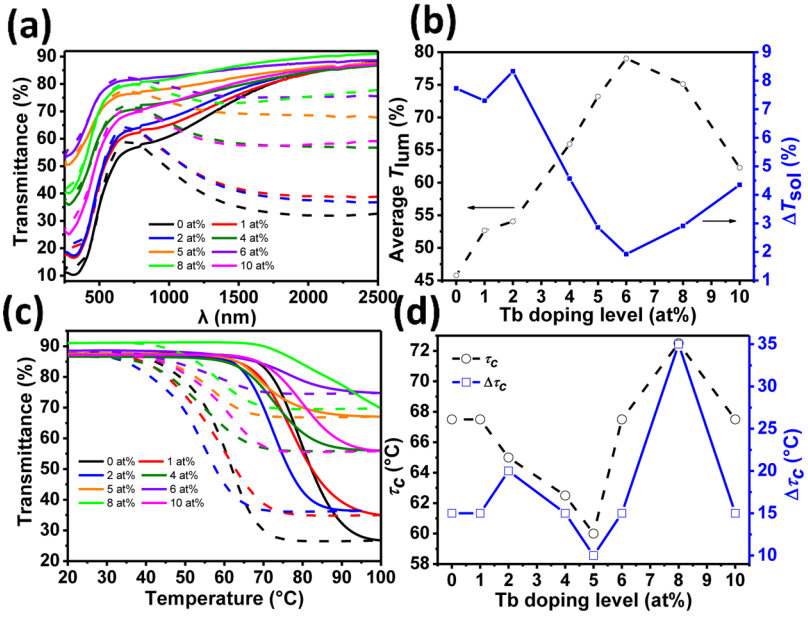

Figure 4. (a) UV−vis−NIR spectra of Tb-doped VO_2 thin films, all collected at 20 °C (solid lines) and 90 °C (dashed lines). (b) Plots of doping level dependent average T_{lum} and ΔT_{sol} for Tb-doped VO_2 thin films. (c) %T hysteresis loops of Tb-doped VO_2 thin films collected at λ = 2500 nm. Solid lines represent the heating processes, and the dashed lines are the cooling curves. (d) Phase transition temperatures (τ_c) and hysteresis loop width ($\Delta\tau_c$) of Tb-doped VO_2 thin films.

DOI: 10.1021/acs.langmuir.5b04212
Langmuir 2016, 32, 759−764

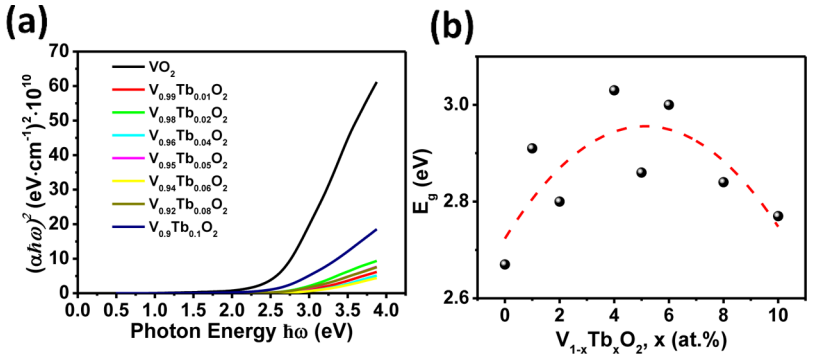

Figure 5. Plots of $(\alpha\hbar\omega)^2$ vs $\hbar\omega$ (a) and the photonic band gap E_g (b) of the VO_2 thin films.

The morphology of the thin films is shown in Figure 2, and the mean particle size was analyzed with NanoScope Analysis 3.0 software ranges approximately from 50 to 80 nm, with the exception of ∼100 nm at 10 at. % Tb doping (Table 2). The measured roughness value ranges from 0.7 to 4.5 nm, and the smoothness would indicate an even distribution of the VO_2 nanoparticles on the fused silica substrates as shown in the 2D images, which may lead to the high average T_{lum} of the samples. The morphology and the phase of VO_2 thin film have been further confirmed by the TEM characterization. As shown in Figure 3, the thin film ($V_{0.98}Tb_{0.02}O_2$) exhibits the average grain size ∼62 nm (Figure 3a), in accordance with the AFM result. The pattern of selected area electron diffraction (SAED, Figure 3b) can be indexed with VO_2 crystalline faces (011), (−211), (−212), and (220). The Tb doping was further confirmed by the HRTEM as shown in Figure 3c, where the larger Tb atoms (pointed by black arrows) could be observed in the lattice distortion region arising from the replacement of V by Tb [ionic radius ratio: 0.92 Å (Tb^{3+}) vs 0.58 Å (V^{4+})]. The EDX mapping, as shown in Figures 3d and 3e, reveals the uniform doping of Tb in the VO_2 thin film.

3.2. Thermochromic Properties. Figure 4a displays the UV−vis−NIR spectra of the samples. It can be observed that as Tb doping level increases, the average T_{lum} is continuously improved from 45.8% (undoped) and capped at 79.0% (6 at. % Tb-doped), after which falling back slightly (Figure 4b and Table 2). Tb doping largely enhances the transmission in both visible and infrared (IR) range at both high and low temperatures. With higher Tb doping level, transmittance contrast at λ = 2500 nm gets smaller, possibly due to the adjustment in crystal structure as a result of introduction of large Tb^{3+} dopant ions. The interference effect between the $\%T$ at low and high temperatures[16] is observed from 0 to 2 at. % Tb doping, where the crossing points of temperature dependent $\%T$ curves show a blue-shift trends along with the RE doping. This could lead to the slight enhancement in ΔT_{sol} from 7.7% to 8.3%. However, when Tb doping level is beyond 2 at. %, the interference effect discontinued and thus ΔT_{sol} shows a backward turning trend (Figure 4b and Table 2). Figure 4b displays the overall trends in average T_{lum} and ΔT_{sol} as functions of Tb doping level. It is interesting to find that 6 at. % Tb-doping is a turning point for both properties, at which average T_{lum} is at maximum while ΔT_{sol} is the lowest. It is worth noting that the phenomenal relative enhancement of T_{lum} of ∼80% at 6 at. % doping level has surpassed the best reported dopings as shown in Table 1. From the data obtained, the overall best combination of thermochromic properties happens at 2 at. % Tb doping; there is an obvious relative enhancement (∼18%) in average T_{lum} compared to the undoped sample, while ΔT_{sol} is also increased slightly from 7.7% to 8.3%. The hysteresis loops of $\%T$ recorded at the wavelength of 2500 nm were formed upon heating and cooling as depicted in Figure 4c, indicating that the MIT is a first-order phase transition. The temperatures at which the sharpest changes happen in both heating and cooling curves are taken from the hysteresis loops as $\tau_{c,heating}/\tau_{c,cooling}$. The average of $\tau_{c,heating}$ and $\tau_{c,cooling}$ represents the τ_c, while the difference ($\Delta\tau_c = \tau_{c,heating} - \tau_{c,cooling}$) is the hysteresis loop width. As tabulated in Table 2, Tb-doping reduces τ_c at a rate of 1.5 °C/at.% up to 5 at. %, after which τ_c returns back to the value of undoped sample (67.5 °C) and even get higher to 72.5 °C at 8 at. % Tb doping (Figure 4d). This might be explained by the competition between the effect of large ionic radius (increasing strain energy) and h^+ carrier density. In other words, the larger ionic radius of Tb^{3+} results in the τ_c reduction at lower doping level (<5 at. %)[30] while the high concentration of h^+ carrier gives rise to the τ_c increment at higher doping level.[31] The τ_c reduction under Tb doping is in accordance with the density functional theory study on doped VO_2 materials with large radius cations.[32] Compared with the reported F-,[33] Mg-,[34] Zr-doped, or W−Zr-codoped VO_2 thin films,[35] the Tb-doped VO_2 exhibits the largest T_{lum} but less ΔT_{sol}.

3.3. Band Gap of the Thin Films. As illustrated in the literature,[36] the optical band gap of semiconductors could be determined according to the expression $(\alpha\hbar\omega)^m = A(\hbar\omega - E_g)$, where m = 1/2, 1/3, 2, and 2/3 represents the indirect-allowed, indirect-forbidden, direct-allowed, and direct-forbidden optical transition, respectively. In addition, the energy gap detected by optical experiment is usually the direct band gap owing to the momentum conservation with low-excitation probability during the optical transition between two different symmetry points.[37] Therefore, we determined the direct band gap of the pristine and doped VO_2 samples by fitting the linear part of the curve $(\alpha\hbar\omega)^2$ vs $\hbar\omega$ (Figure 5a) with the expression $(\alpha\hbar\omega)^2 = A(\hbar\omega - E_g)$, where α is the absorption coefficient ($\alpha d = -\ln(T/1 - R)$), A is a constant, and $\hbar\omega$ is the photon energy. As depicted in Figure 5b, the E_g is widened steadily from 2.67 to 3.0 eV along with the Tb doping (below 6 at. %), which should benefit the increase of T_{lum} as seen in Table 2. Such similar behavior has also been reported in Mg^{2+}-doped VO_2 thin films.[38−41] However, upon further increasing the Tb doping, the E_g begins to decay slightly, resulting in a moderately drop of T_{lum}, which may be ascribed to the competition between the strain energy and the h^+ carrier density introduced by the Tb^{3+} doping.

DOI: 10.1021/acs.langmuir.5b04212
Langmuir 2016, 32, 759−764

4. CONCLUSIONS

In summary, the Tb^{3+} cations were first doped into the VO_2 lattice, and an enhancement of thermochromic properties in terms of reduced τ_c and largely increased T_{lum} was observed at the doping level from 1 to 5 at. %. With Tb^{3+} doping from 1 to 5 at. %, the T_{lum} was largely increased from 45.8% (pristine VO_2) to 73.2% while τ_c was marginally reduced from 67.5 °C (pristine VO_2) to 60 °C. However, upon further increasing the doping level to 10 at. %, the T_{lum} was slightly depressed to 62.8% and the τ_c returned back to 67.5 °C, which should be mainly ascribed to the competition between the strain energy and the free h^+ carrier density introduced by the doping. With regard to the smart window applications, the future study on Tb−M (M = W, Mg, F, Zr)-codoped VO_2 thin films may provide an alternative way to get a combination of high T_{lum} as well as large ΔT_{sol}, considering the increase of T_{lum} with slightly compromised ΔT_{sol} in single Tb doping.

AUTHOR INFORMATION

Corresponding Author

*E-mail longyi@ntu.edu.sg; Tel +65 67904599; Fax +65 67911604 (Y.L.).

Notes

The authors declare no competing financial interest.

ACKNOWLEDGMENTS

This research is supported by the Singapore National Research Foundation under CREATE programme: Nanomaterials for Energy and Water Management and Singapore Ministry of Education (MOE) Academic Research Fund Tier 1 RG101/13 and an MSE-ERC Julich collaboration-MAP project grant. XRD, FESEM and TEM characterization was performed at the Facility for Analysis, Characterization, Testing and Simulation (FACTS) in Nanyang Technological University, Singapore and in the Ernst Ruska-Centre for Microscopy and Spectroscopy with Electrons (ER-C) in Forschungszentrum Jülich, Germany. The authors acknowledge financial support from the European Union under the Seventh Framework Programme under a contract for an Integrated Infrastructure Initiative. Reference 312483-ESTEEM2. In addition, we thank Mr Min Hao Goh for the XPS test.

REFERENCES

(1) Qazilbash, M. M.; Brehm, M.; Chae, B.-G.; Ho, P.-C.; Andreev, G. O.; Kim, B.-J.; Yun, S. J.; Balatsky, A. V.; Maple, M. B.; Keilmann, F.; Kim, H.-T.; Basov, D. N. Mott Transition in VO_2 Revealed by Infrared Spectroscopy and Nano-Imaging. *Science* **2007**, *318*, 1750−1753.

(2) Liu, M. K.; Hwang, H. Y.; Tao, H.; Strikwerda, A. C.; Fan, K. B.; Keiser, G. R.; Sternbach, A. J.; West, K. G.; Kittiwatanakul, S.; Lu, J. W.; Wolf, S. A.; Omenetto, F. G.; Zhang, X.; Nelson, K. A.; Averitt, R. D. Terahertz-field-induced insulator-to-metal transition in vanadium dioxide metamaterial. *Nature* **2012**, *487*, 345−348.

(3) Zhou, Y.; Cai, Y.; Hu, X.; Long, Y. Temperature-responsive hydrogel with ultra-large solar modulation and high luminous transmission for "smart window" applications. *J. Mater. Chem. A* **2014**, *2*, 13550−13555.

(4) Zhou, Y.; Cai, Y.; Hu, X.; Long, Y. VO_2/hydrogel hybrid nanothermochromic material with ultra-high solar modulation and luminous transmission. *J. Mater. Chem. A* **2015**, *3*, 1121−1126.

(5) Wang, N.; Magdassi, S.; Mandler, D.; Long, Y. Simple sol−gel process and one-step annealing of vanadium dioxide thin films: Synthesis and thermochromic properties. *Thin Solid Films* **2013**, *534*, 594−598.

(6) Wang, N.; Huang, Y.; Magdassi, S.; Mandler, D.; Liu, H.; Long, Y. Formation of VO_2 zero-dimensional/nanoporous layers with large supercooling effects and enhanced thermochromic properties. *RSC Adv.* **2013**, *3*, 7124−7128.

(7) Liu, C.; Wang, N.; Long, Y. Multifunctional overcoats on vanadium dioxide thermochromic thin films with enhanced luminous transmission and solar modulation, hydrophobicity and anti-oxidation. *Appl. Surf. Sci.* **2013**, *283*, 222−226.

(8) Boscolo, A.; Menosso, E.; Piuzzi, B.; Toppano, M. Thermocromic Materials for Temperature Sensors in New Applications. In *Device Applications of Nonlinear Dynamics*; Baglio, S., Bulsara, A., Eds.; Springer: Berlin, 2006; pp 139−144.

(9) Jorgenson, G. V.; Lee, J. C. Doped vanadium oxide for optical switching films. *Sol. Energy Mater.* **1986**, *14*, 205−214.

(10) Chain, E. E. Optical properties of vanadium dioxide and vanadium pentoxide thin films. *Appl. Opt.* **1991**, *30*, 2782−2787.

(11) Chen, S.; Dai, L.; Liu, J.; Gao, Y.; Liu, X.; Chen, Z.; Zhou, J.; Cao, C.; Han, P.; Luo, H.; Kanahira, M. The visible transmittance and solar modulation ability of VO_2 flexible foils simultaneously improved by Ti doping: an optimization and first principle study. *Phys. Chem. Chem. Phys.* **2013**, *15*, 17537−17543.

(12) Strelcov, E.; Lilach, Y.; Kolmakov, A. Gas Sensor Based on Metal−Insulator Transition in VO_2 Nanowire Thermistor. *Nano Lett.* **2009**, *9*, 2322−2326.

(13) Liu, C.; Cao, X.; Kamyshny, A.; Law, J. Y.; Magdassi, S.; Long, Y. VO_2/Si−Al gel nanocomposite thermochromic smart foils: Largely enhanced luminous transmittance and solar modulation. *J. Colloid Interface Sci.* **2014**, *427*, 49−53.

(14) Chen, Z.; Gao, Y.; Kang, L.; Cao, C.; Chen, S.; Luo, H. Fine crystalline VO_2 nanoparticles: synthesis, abnormal phase transition temperatures and excellent optical properties of a derived VO_2 nanocomposite foil. *J. Mater. Chem. A* **2014**, *2*, 2718−2727.

(15) Qian, X.; Wang, N.; Li, Y.; Zhang, J.; Xu, Z.; Long, Y. Bioinspired Multifunctional Vanadium Dioxide: Improved Thermochromism and Hydrophobicity. *Langmuir* **2014**, *30*, 10766−10771.

(16) Cao, X.; Wang, N.; Law, J. Y.; Loo, S. C. J.; Magdassi, S.; Long, Y. Nanoporous Thermochromic VO_2 (M) Thin Films: Controlled Porosity, Largely Enhanced Luminous Transmittance and Solar Modulating Ability. *Langmuir* **2014**, *30*, 1710−1715.

(17) Cao, X.; Wang, N.; Magdassi, S.; Mandler, D.; Long, Y. Europium Doped Vanadium Dioxide Material: Reduced Phase Transition Temperature, Enhanced Luminous Transmittance and Solar Modulation. *Sci. Adv. Mater.* **2014**, *6*, 558−561.

(18) Mlyuka, N. R.; Niklasson, G. A.; Granqvist, C. G. Mg doping of thermochromic VO_2 films enhances the optical transmittance and decreases the metal-insulator transition temperature. *Appl. Phys. Lett.* **2009**, *95*, 171909.

(19) Li, S.-Y.; Niklasson, G. A.; Granqvist, C. G. Nanothermochromics: Calculations for VO_2 nanoparticles in dielectric hosts show much improved luminous transmittance and solar energy transmittance modulation. *J. Appl. Phys.* **2010**, *108*, 063525.

(20) Li, S.-Y.; Niklasson, G. A.; Granqvist, C. G. Nanothermochromics with VO_2-based core-shell structures: Calculated luminous and solar optical properties. *J. Appl. Phys.* **2011**, *109*, 113515.

(21) Burkhar dt, W.; Christmann, T.; Franke, S.; Kriegseis, W.; Meister, D.; Meyer, B. K.; Niessner, W.; Schalch, D.; Scharmann, A. Tungsten and fluorine co-doping of VO_2 films. *Thin Solid Films* **2002**, *402*, 226−231.

(22) Batista, C.; Ribeiro, R. M.; Teixeira, V. Synthesis and characterization of VO_2-based thermochromic thin films for energy-efficient windows. *Nanoscale Res. Lett.* **2011**, *6*, 301.

(23) Ufert, K.-D. Doping of VO_2 Thin Films by Ion Implantation. *phys. stat. sol. (a)* **1977**, *42*, 187−190.

(24) Phillips, T. E.; Murphy, R. A.; Poehler, T. O. Electrical Studies of Reactively Sputtered Fe-Doped VO_2 Thin Films. *Mater. Res. Bull.* **1987**, *22*, 1113−1123.

(25) Gao, Y.; Cao, C.; Dai, L.; Luo, H.; Kanehira, M.; Ding, Y.; Wang, Z. L. Phase and shape controlled VO_2 nanostructures by antimony doping. *Energy Environ. Sci.* **2012**, *5*, 8708.

DOI: 10.1021/acs.langmuir.5b04212
Langmuir 2016, 32, 759−764

(26) Du, J.; Gao, Y.; Luo, H.; Zhang, Z.; Kang, L.; Chen, Z. Formation and metal-to-insulator transition properties of VO_2−ZrV_2O_7 composite films by polymer-assisted deposition. *Sol. Energy Mater. Sol. Cells* **2011**, *95*, 1604−1609.
(27) Cao, J.; Ertekin, E.; Srinivasan, V.; Fan, W.; Huang, S.; Zheng, H.; Yim, J. W. L.; Khanal, D. R.; Ogletree, D. F.; Grossmanan, J. C.; Wu, J. Strain engineering and one-dimensional organization of metal-insulator domains in single-crystal vanadium dioxide beams. *Nat. Nanotechnol.* **2009**, *4*, 732−737.
(28) Wyszecki, G.; Stiles, W. S. *Color Science: Concepts and Methods, Quantative Data and Fomulae*, 2nd ed.; Wiley: New York, 2000.
(29) ASTM G173-03 Standard Tables of Reference Solar Spectral Irradiances: Direct Normal and Hemispherical on a 37° Tilted Surface. Annual Book of ASTM Standards American Society for Testing and Materials, Philadelphia, PA, 2003.
(30) Kiri, P.; Hyett, G.; Binions, R. Solid state thermochromic materials. *Adv. Mater. Lett.* **2010**, *1*, 86−105.
(31) Goodenough, J. B. The Two Components of the Crystallographic Transition in VO_2. *J. Solid State Chem.* **1971**, *3*, 490−500.
(32) Sun, C.; Yan, L.; Yue, B.; Liu, H.; Gao, Y. The modulation of metal-insulator transition temperature of vanadium dioxide: a density functional theory study. *J. Mater. Chem. C* **2014**, *2*, 9283−9293.
(33) Dai, L.; Chen, S.; Liu, J.; Gao, Y.; Zhou, J.; Chen, Z.; Cao, C.; Luo, H.; Kanehira, M. F-doped VO_2 nanoparticles for thermochromic energy-saving foils with modified color and enhanced solar-heat shielding ability. *Phys. Chem. Chem. Phys.* **2013**, *15*, 11723−11729.
(34) Zhou, J.; Gao, Y.; Liu, X.; Chen, Z.; Dai, L.; Cao, C.; Luo, H.; Kanahira, M.; Sun, C.; Yan, L. Mg-doped VO_2 nanoparticles: hydrothermal synthesis, enhanced visible transmittance and decreased metal-insulator transition temperature. *Phys. Chem. Chem. Phys.* **2013**, *15*, 7505−7511.
(35) Shen, N.; Chen, S.; Chen, Z.; Liu, X.; Cao, C.; Dong, B.; Luo, H.; Liu, J.; Gao, Y. The synthesis and performance of Zr-doped and W-Zr-codoped VO_2 nanoparticles and derived flexible foils. *J. Mater. Chem. A* **2014**, *2*, 15087−15093.
(36) Tauc, J.; Menth, A. States in the gap. *J. Non-Cryst. Solids* **1972**, *8*−*10*, 569−585.
(37) Liu, G.-H.; Deng, X.-Y.; Wen, R. Electronic and optical properties of monoclinic and rutile vanadium dioxide. *J. Mater. Sci.* **2010**, *45*, 3270−3275.
(38) Li, S.-Y.; Mlyuka, N. R.; Primetzhofer, D.; Hallén, A.; Possnert, G.; Niklasson, G. A.; Granqvist, C. G. Bandgap widening in thermochromic Mg-doped VO_2 thin films: Quantitative data based on optical absorption. *Appl. Phys. Lett.* **2013**, *103*, 161907.
(39) Li, S. Y.; Niklasson, G. A.; Granqvist, C. G. Thermochromic fenestration with VO_2-based materials: Three challenges and how they can be met. *Thin Solid Films* **2012**, *520*, 3823−3828.
(40) Hu, S.; Li, S. Y.; Ahuja, R.; Granqvist, C. G.; Hermansson, K.; Niklasson, G. A.; Scheicher, R. H. Optical properties of Mg-doped VO_2: Absorption measurements and hybrid functional calculations. *Appl. Phys. Lett.* **2012**, *101*, 201902.
(41) Gagaoudakis, E.; Kortidis, I.; Michail, G.; Tsagaraki, K.; Binas, V.; Kiriakidis, G.; Aperathitis, E. Study of low temperature rf-sputtered Mg-doped vanadium dioxide thermochromic films deposited on low-emissivity substrates. *Thin Solid Films* **2015**, in press.

DOI: 10.1021/acs.langmuir.5b04212
Langmuir 2016, 32, 759−764